SYNOPTIC FEATURES ASSOCIATED WITH TEMPORALLY COHERENT MODES OF VARIABILITY OF THE NORTH PACIFIC JET STREAM

Kyle S. Griffin and Jonathan E. Martin

Department of Atmospheric and Oceanic Sciences, University of Wisconsin-Madison

Corresponding author address: *J. E. Martin,*
1225 W. Dayton Street, Madison WI, 53706
Email: jemarti1@wisc.edu

Submitted to *Journal of Climate*, 20 November 2015

Abstract

Time extended EOF (TE-EOF) analysis is employed to examine the synoptic-scale evolution of the two leading modes of the north Pacific jet stream variability, namely its zonal extension/retraction and the north/south shift of its exit region. Use of the TE-EOF analysis enables a temporally coherent examination of the synoptic-scale evolution preceding and following times of peak variability of each mode that provides a novel perspective on the preferred evolutions of the north Pacific jet.

Composite analyses are constructed based upon selecting peaks with magnitude in excess of 1.5 sigma in the principal component time series of both phases of each TE-EOF. An anomalous Gulf of Alaska cyclone that induces a low-level warm anomaly over western North America is associated with jet extensions. Jet retractions are associated with a nearly opposite evolution characterized by an anomalous ridge over the Aleutians and anomalous low-level cold over western North America. Similar but lower-amplitude upper level patterns are noted in the composites of the corresponding TE-EOF 2 phases, with the poleward shift of the jet exit region tied to an anomalous Alaskan cyclone and anomalous low-level warmth over north central North America. An equatorward shift of the exit region is tied to an anomalous Alaskan ridge with downstream cold anomalies occurring in western North America. The more extreme downstream impacts that characterize TE-EOF 2 are also longer lasting (>5 days), suggesting potential utility in medium-range forecasts.

1. Introduction

Among the most ubiquitous structural characteristics of the Earth's atmosphere are the narrow, rapidly flowing currents of air located near the tropopause, known as jet streams or jets. These synoptic features were largely unknown before and during World War II despite their original identification by Wasaburo Ooishi over Japan in 1924 (Lewis 2003). By the end of the war, however, the existence of jet streams was well established, quickly drawing substantial amounts of research attention that led to the discovery of the separate subtropical (e.g. Loewe and Radok 1950, Yeh 1950, Koteswaram 1953) and polar (e.g. Namias and Clapp 1944, Palmén 1951, Newton 1954) jets.

The first comprehensive descriptions of north Pacific jet stream structure were provided by Mohri (1953). He emphasized that the jet sat between contrasting air masses and that what often appeared to be a single jet entity was, in fact, a hybrid of the separate subtropical and polar jets. Considerable attention has been directed toward understanding the influence of external processes on the evolution of the jet. For instance, deep tropical convection, organized on the synoptic-scale, can impact the jet either directly via upper-level divergent outflow or remotely through amplification of the ambient mid-latitude flow (e.g. Kiladis and Weickmann 1992, Madden and Julian 1994, Higgins et al. 2000, Archambault et al. 2013).

To date, the inherent variability of the north Pacific jet and its resultant impacts on the regional and hemispheric flow have been less thoroughly investigated. Schubert and Park (1991) conducted one of the first examinations of the intraseasonal variability of the North Pacific jet by performing an empirical

orthogonal function (EOF) analysis on zonal wind filtered for a 20-70 day period. The leading mode of variability associated with this EOF analysis described a modulation of the zonal wind intensity in the core of the North Pacific jet, while the second leading mode of variability described a modulation of the zonal extent of the jet. Eichelberger and Hartmann (2007) further highlighted the important role played by the modulation of the zonal extent of the jet in explaining jet variability over the North Pacific in their investigation of zonal mean jet structures. They attributed one of their analyzed modes of variability to a combination of a north-south shift, pulsing intensity, and extension/retraction of the jet stream over the North Pacific, portraying the variability of the jet on the synoptic scale to be significantly more complicated than that revealed in the analysis of Schubert and Park (1991).

Among the earliest study to note the regional impacts of inter-seasonal variability of the north Pacific jet was that of Chu et al. (1993). They showed that differences in the zonal extent of the jet had an enormous impact on rainfall in Hawaii as a zonally retracted (extended) jet in 1982-83 (1981-82) was associated with an extremely wet (dry) winter. Otkin and Martin (2004) constructed a synoptic climatology of Kona low frequency near Hawaii using 10 years of ECMWF Tropical Ocean Global Atmosphere (TOGA) surface and upper-air data. They found that a retracted jet was associated with increased Kona low frequency in the central Pacific, suggesting that with the jet exit region retracted west of the dateline (its climatological position) the waveguide was absent north of the Hawaiian Islands,

consequently allowing unimpeded equatorward propagation of extratropical disturbances to the subtropics in that longitude sector.

More recently, studies undertaken by Athanasiadis et al. (2010) and Jaffe et al. (2011) identified two leading modes of variability of the north Pacific jet. Both studies employed EOF analysis of unfiltered zonal wind data and found the leading mode consists of a longitudinal shift of the north Pacific jet exit region such that in the extended phase (EOF 1+) the jet may reach as far eastward as the western coast of North America, while in the retracted phase (EOF 1-) the jet may extend only as far as 160°E. The second mode highlights a 10-15° meridional shift in the jet exit region (EOF 2+, a northward shift; EOF 2-, an equatorward shift). Jaffe et al. (2011) also investigated the synoptic evolution of sudden jet retractions and found the characteristic timescale for such events was ~10 days.

Thus, of the four characteristic north Pacific jet configurations associated with the leading two modes of variability (EOF 1+, EOF 1-, EOF 2+, and EOF 2-), only the synoptic-evolution of jet retractions (EOF 1-) has been investigated. That investigation (by Jaffe et al. 2011) was undertaken via compositing around a single time of maximum jet retraction intensity. Employment of such a method limits the ability of the composite to 1) testify to conditions spatially or temporally removed from the central region of interest and 2) capture the temporal evolution of associated large- and synoptic-scale structures.

In order to extend the perspective gained from compositing techniques and improve signal retention at longer time lags, a more robust method of identifying and describing the evolution of the jet stream structure is required. This paper

adapts the extended EOF methodology (e.g. Weare and Nasstrom 1982, Wilks 2011) to examine the synoptic evolution of temporally coherent structures characterizing the leading modes of north Pacific jet variability. A description of the time-extended EOF (TE-EOF) method, along with details of its implementation in this study, is discussed as part of a broader description of the methodology in Section 2. Section 3 describes the jet variability on synoptic timescales within the TE-EOF framework. Time-lagged composites, constructed based on data from the TE-EOF analysis, highlighting synoptic features locally over the North Pacific as well as associated high-impact effects downstream over North America, are presented in section 4. Additional time-lagged composites of anomalous deep convection are constructed via the same methodology and presented in section 5. A summary and suggestions for future work are discussed in section 6.

2. Methodology

EOF analysis is a statistical method by which the recurring patterns describing a multi-dimensional dataset are identified (e.g. Hannachi 2004, Wilks 2011). The patterns of greatest interest in an EOF analysis are those that explain the largest fraction of variability within that dataset. In the atmosphere, EOF analyses provide insight into the primary modes of variability associated with a particular atmospheric variable over a pre-defined spatial region and period of time. Use of EOF analyses has led to the identification and analysis of large-scale patterns in the atmosphere (e.g. the PNA, Wallace and Gutzler 1981; AO, Thompson and Wallace 1998), although not all EOFs have a corresponding physical interpretation. Given

142 that each mode of variability identified by an EOF analysis is defined to be
143 statistically independent of all other modes, changes in any one mode have no
144 correlation with changes in any other mode. In actual complex systems, such as the
145 atmosphere, the asserted mathematical independence of each mode need not be
146 mirrored in reality. However, when physical insight is combined with the statistical
147 results of EOF analyses, the combined analysis can lead to understanding that
148 neither the physics nor statistics might provide alone.

149 The traditional EOF analyzes a temporal sequence of spatial information to
150 determine patterns of spatial variability without providing any sense of how such a
151 pattern may evolve through time. By extending the input data to include a temporal
152 dimension, EOF analysis can identify the time-dependent evolution of spatial
153 patterns. This particular extended EOF (Weare and Nasstrom 1982, Wilks 2011) has
154 been termed a time-extended EOF (TE-EOF; Roundy and Schreck 2009) and
155 describes the leading modes of spatial-temporal evolution for the analyzed data. TE-
156 EOF incorporates temporal variability by considering a number of times either side
157 of a central reference time. By doing so, temporal data is incorporated into the TE-
158 EOF twice – once as a way to maintain the coherence of data related to the evolution
159 of the pattern over a, for instance, 10-day window (the additional TE-EOF
160 dimension, termed a "TE window") and once as the time series over which to
161 calculate the eigenmodes and identify the historical patterns associated with each
162 mode of variability. Weare and Nasstrom (1982) introduced the concept of
163 extended EOF analysis in the atmospheric sciences and emphasized the utility of
164 extended EOFs that incorporate additional temporal data due to the "significant

auto- and cross-correlations in time" associated with atmospheric data. Extended EOFs have been utilized to produce multivariate extended EOF analyses (including multiple variables instead of multiple times), such as those used by Wheeler and Hendon (2004) to monitor the Madden-Julian Oscillation, and the time-extended EOF analyses used to forecast organized modes of tropical convection by Roundy and Schreck (2009).

The TE-EOF analyses performed in this study were constructed with data from the NCEP/NCAR Reanalysis (Kalnay et al. 1996) with data at 2.5° horizontal grid spacing and 6-hourly resolution. Zonal wind at the 250-hPa level was used at each analysis time throughout the winter months of November – March (NDJFM). The chosen spatial domain of 100°E–120°W and 10°N–80°N allows sufficient space around the entrance and exit regions of the North Pacific (NPAC) jet stream in order to fully capture the variability directly associated with each. The TE-EOFs are performed using a TE-window of 40 time steps (10 days) of zonal wind anomalies beginning at each 6-hourly time step during NDJFM. These times are buffered by 5 days at the beginning of November and end of March to include only TE windows that fall completely within the NDJFM period. For example, the first (second) TE window in this analysis extends from 0000 UTC 1 Nov to 1800 UTC 10 Nov (0600 UTC 1 Nov to 0000 UTC 11 Nov) and is represented by the central time of 0000 UTC 5 Nov (0600 UTC 5 Nov).

In constructing the TE-EOF analyses, tests were performed to examine the sensitivity of the resulting TE-EOF 1 and TE-EOF 2 patterns to the chosen temporal and spatial constraints on the domain. Given the broad similarity of DJF and NDJFM

188 zonal wind EOFs (not shown), and in order to reduce calculation time, the TE-EOFs
189 for the sensitivity tests were calculated only over the DJF period. To test temporal
190 constraints, the TE window length was varied from 6 days to 16 days, showing only
191 minor changes in the TE-EOF patterns. Numerous variations of the spatial domain
192 were tested. Expansions of the domain captured the high zonal wind variability
193 associated with other climatological jet streams over central Asia and eastern North
194 America, but did not significantly impact the pattern in the area of interest over the
195 North Pacific. The spatial dimensions of the domain specified above were therefore
196 chosen to focus on variability of the North Pacific jet while excluding other remote
197 regions of high zonal wind variability.

198 The utility of the TE methodology is evident when comparing the resultant
199 principal components (PCs) to the PCs of a traditional EOF analysis on the same
200 data. PCs represent a measure of how well the data at a given time projects back
201 onto a given mode of variability. A time series of PCs provides a running measure of
202 this projection and is standardized to aid interpretation. For the NDJFM months of
203 2009-2010, Fig. 1 compares the TE-PC (from a 10-day TE window) to the traditional
204 PC (instantaneous; calculated every 6 h) and the 10-day centered running mean of
205 the traditional PC. While the traditional PC captures more variability in the state of
206 the North Pacific jet stream on short time scales, this variability has no inherent
207 regard for maintaining the temporal coherence of the PC and can appear noisy at
208 times. Smoothing the traditional PC time series over 40 points (10 days) provides
209 values that appear similar to, but are generally of smaller magnitude than, the TE-PC
210 values. As a result, the TE-PC better captures the full magnitude of highly anomalous

events on the 10-day timescale while eliminating much of the noise from higher-frequency variability, facilitating a focus on events on the synoptic time scale. While Fig. 1 contains data only for the 2009-2010 NDJFM season, similar comparisons hold across all winters since 1980-1981 and suggest the TE methodology is better suited than the traditional or smoothed PCs for identifying intraseasonal shifts in the structure of the North Pacific jet stream.

It is important to note that the TE modes are defined in a manner that does not require that peaks in a PC from a traditional EOF technique correspond to peaks in a mode from the TE-PC. The TE-PC captures the broader evolution of the pattern without accounting for higher-frequency signals that may project onto the traditional EOF patterns yet lack temporal longevity. It is likely these types of peaks in the PC are not captured by the TE-EOF, and in turn may account for some of the lower percent of variance explained with each TE mode when compared to the corresponding traditional EOF over the north Pacific region[1]. Such a reduction in explained variance by a given TE-EOF is related to the larger number of data points employed in the construction of the TE-EOF (Weare and Nasstrom 1982).

In order to supplement the TE-EOF analysis of the zonal wind field with physical analysis, composite analyses of high-amplitude events in the PC time series between November and March for the years 1980–2010 were constructed with anomalies calculated from a climatology utilizing 21-day centered running means from the NCEP/NCAR Reanalysis (Kalnay et al. 1996). Such composites allow for an

[1] The percent variance explained in Jaffe et al. (2011) for EOF 1 is 15.9%, compared to our 9.1%. Our TE-EOFs are calculated using approximately 40 times the number of data points than used in a traditional EOF analysis.

examination of the synoptic-scale patterns preceding and following high-amplitude peaks in given modes of jet stream variability. In addition, outgoing longwave radiation (OLR) anomalies from the NOAA Interpolated OLR dataset (Liebmann and Smith 1996; provided by the NOAA/OAR/ESRL PSD, Boulder, Colorado, USA, for 1979–2012 from http://www.esrl.noaa.gov/psd/) were utilized in constructing additional composite analyses and serve as a reasonable proxy for anomalous cloud cover and convection in the tropics and subtropics. In these composites, D0 will refer to date and time where a local maximum (or minimum) in the given PC exceeded the prescribed threshold, while D-5d and D+5d will refer to the dates five days prior to and five days following D0, respectively.

3. Preferred modes of variability

The TE-EOF analyses presented here remain consistent with the leading modes of jet stream variability identified by previous work while capturing the broader temporal evolution of synoptic-timescale patterns in the north Pacific jet stream. Previous work has shown the spatial patterns associated with the leading modes of variability of the zonal wind over the north Pacific (e.g. Fig. 4 of Athanasiadis et al. 2010, Fig. 4 of Jaffe et al. 2011) to be similar to the patterns associated with the two leading modes of variability found at the central day (D0) of the TE window used in the TE-EOF analysis as shown in Fig. 2 (EOF 1) and Fig. 3 (EOF 2). The two other panels of Figs. 2 and 3, labeled as D-5d and D+5d, represent the beginning and end of the TE window, respectively. It is important to recognize that the sign associated with any EOF analysis is arbitrary and the signs of the TE-

EOFs presented here have been chosen in a manner consistent with previous literature.

TE-EOF 1 is comprised of zonal wind variability along the latitude of the climatological jet core (~35°N), with a maximum variability of the mode located in the exit region of the climatological jet. Figure 2 presents the anomalies from the NCEP/NCAR Reanalysis regressed back onto the TE-EOF pattern, resulting in a maximum anomaly in excess of 24 m s^{-1} at D0 (Fig. 2b). This anomaly represents the extension (when positive) and retraction (when negative) events of the north Pacific jet characterized by TE-EOF 1. A second set of anomalies of the opposite sign can be found both poleward and equatorward of the maximum anomaly in the jet exit region. In general, the large-scale TE-EOF anomalies maximize in intensity near the central point of the 10-day TE window.

TE-EOF 2 represents a meridional shift in the exit region of the climatological jet stream, described by a pair of anomalies of opposing sign straddling the climatological latitude of the jet stream (Fig. 3). Such a pattern indicates a shift of the zonal wind to the flank of the climatological jet exit region. The northern (southern) anomaly center, when positive, represents a poleward (equatorward) shift in the jet exit region. These distinct shifts correspond, respectively, to the positive and negative phases of TE-EOF 2.

4. Composite analysis

In order to provide insight into the evolution of the synoptic-scale patterns associated with each sign of the two modes of variability, four separate composites

were constructed. Each instance in which a given PC's value reached a local maxima or minima in excess of ±1.5 standard deviations was selected for the composite. Anomaly data from upper (250 hPa) and lower (850 hPa) levels at the selected times were averaged to produce each composite. The same NCEP/NCAR Reanalysis anomaly data used to originally construct the TE-EOFs was also employed in the construction of the composites.

a. Extension (positive TE-EOF 1)

The composite analysis of TE-EOF 1 in its positive phase, created from 40 individual maxima in the PC of TE-EOF 1, is presented in Figure 4. When in its positive phase, TE-EOF 1 represents an extension of the climatological jet over the north Pacific, with the strongest zonal wind anomaly at D0 located near 35˚N and 165˚W (Fig. 4c), firmly embedded within the exit region of the climatological jet. At upper levels (Fig. 4a), a modest 15 m s^{-1} anomaly is found at D-5d extending from 150˚E to 140˚W equatorward of an anomalous upper level trough and associated low-level anomalous cyclone (Fig. 4b) south of the Aleutian Islands. This low-level cyclone is supported at upper levels by the extended jet to the south, placing the cyclone in the poleward exit region of the jet, a region favorable for cyclone development.

Near the Asian coast at D-5d (Fig. 4a), an anomalous upper level trough supports an enhancement of the low-latitude upper level jet, increasing flow out of the tropics. Over time, this trough fades and merges with the broader trough in the north central Pacific (Fig. 4c, e). There, the anomalous height differential of over 300

m between 20˚N and 40˚N peaks at D0 and is made manifest as a zonal wind anomaly of ~30 m s^{-1}, effectively doubling the zonal wind in this jet exit region (Fig. 4c). The enhancement of the zonal wind in the jet exit region extends the climatological jet 20˚ farther east, approaching the west coast of North America. This jet naturally follows the southern edge of the anomalously low heights associated with the central Pacific trough. Beneath the upper trough, the 850-hPa cyclone continues to develop (-180 m minimum height anomaly) and maintains its position in the poleward exit region of the extended jet as both shift eastward (Fig. 4d). By D+5d, the upper trough remains sprawling and moves the jet even farther east (Fig. 4e). Accordingly, the anomalous 850 hPa cyclone begins to shift onshore over western North America (Fig. 4f), indicating the low-level cyclone is increasingly impacting the sensible weather over North America.

It is interesting to note that the height and zonal wind anomalies over eastern Asia at D-5d, particularly those tied to the ridge over central Siberia and the trough over the Korean peninsula, weaken through D0 and are essentially absent by D+5d. Given that the intensity of each peaks early in the TE window, it may be that these two features identify precursors to jet extension events over the north Pacific. This upper-level trough and ridge are also represented in the 850 hPa temperature anomalies, with anomalous warmth over central Siberia and anomalous cold (in excess of -3˚C) over eastern China at D-5d (Fig. 4b).

Downstream over North America, height anomalies start to amplify by D0, with an anomalous 250 hPa ridge over western Canada (Fig. 4c) associated with widespread 850 hPa temperature anomalies in excess of 2˚C (Fig. 4d). Farther

downstream over the eastern portion of the United States and maritime Canada, an upper-level trough develops with associated low-level cold anomalies in excess of -2˚C at D0. This trough over eastern North America forces a slight enhancement of the upper jet on its equatorward edge in association with negative height anomalies, resulting in a stronger subtropical jet over the southeast United States. While the upper trough and low-level cold anomalies slowly slide southeastward through D+5d, the warm anomalies over western Canada intensify and expand over much of the western half of North America, peaking in excess of 4˚C (Fig. 4f). This warmth appears to last beyond the end of the 10-day TE window analyzed in this composite (not shown), suggesting high-amplitude North American impacts beyond what is described here.

b. Retraction (negative TE-EOF 1)

While composites associated with the negative phase of TE-EOF 1 are not statistically required to be mirror opposites of the positive phase of TE-EOF 1, the large-scale structures describing the two phases tend to exhibit this characteristic. For the jet retraction cases associated with the negative phase of TE-EOF 1, the composite analysis was again constructed from 40 times in which the PC peaked below the -1.5 standard deviation threshold. The composite maps are presented in Figure 5.

At upper levels at D-5d (Fig. 5a), the core of the negative zonal wind anomalies is located near 180˚, placing it within the exit region of the climatological jet and resulting in a weaker, retracted jet whose zonal extent is limited to areas

347 west of the date line. Negative zonal wind anomalies peak in excess of -30 m s^{-1} with
348 these cases (Fig. 5c) in a region where the climatological wind is only ~45 m s^{-1}.
349 Centers of enhanced zonal winds exist both poleward and equatorward of the
350 climatological jet stream with the positive zonal wind anomaly stronger on the
351 poleward side of the climatological jet. A modest upper-level trough appears west of
352 Hawaii (around 180°W; Fig. 5a) and exists throughout the 10-day TE window,
353 expanding eastward with time. Anomalous cyclonic flow around this upper trough
354 further supports the reduction in climatological westerlies in combination with the
355 much more substantial high-latitude ridge farther north, creating a pattern akin to a
356 Rex block (Rex 1950) and suggesting a stagnation of the pattern over the eastern
357 north Pacific and downstream. With the retraction of the jet stream to the west of
358 the blocking pattern, the absence of a mid-latitude waveguide allows for more
359 frequent poleward propagation of tropical air masses and equatorward propagation
360 of polar air masses (e.g. Otkin and Martin 2004).

361 East Asian precursors are comparable but roughly opposite of those of the jet
362 extension mode. Most of Siberia is dominated by a sprawling upper-level trough and
363 low-level cold anomalies (below -4°C), while east-central China and the Sea of Japan
364 are dominated by a western lobe of the ridge in the central Pacific that slowly
365 contracts eastward with time in the 10-day TE window (Fig. 5a, c, e). The
366 anomalously cold air, largely in Siberia initially, spreads eastward to encompass
367 Alaska and western Canada where anomalous cold exceeds -5°C by D0 (Fig. 5d).
368 Simultaneously in Asia, this cold air slides southward into eastern China, with an

East Asian Winter Monsoon (EAWM; Chang and Lau 1980) cold surge signature along the higher terrain of the Tibetan Plateau at D0 (Fig. 5d).

The downstream patterns are of similar amplitude and evolve comparably to those observed in jet extension composites, but are again of reversed sign. A broad region of anomalously low heights at 850 hPa can be seen sliding out of the Arctic Ocean around D0 (Fig. 5d) and into western Canada by D+5 (Fig. 5f), enhancing southerly flow over central North America and amplifying the warm 850 hPa temperature anomalies over the eastern half of North America by D+9d (not shown). Cold air also builds up over northwestern North America, especially during and after peak retraction of the jet over the North Pacific (D+5d and beyond, not shown).

c. Poleward shift (positive TE-EOF 2)

Two primary centers of variability straddling the mean jet exit region dominate the 10-day composite analyses of 36 poleward shifted jet cases (positive phase of TE-EOF 2). A strip of positive zonal wind anomalies north of the climatological jet axis and negative anomalies south of the climatological jet axis serves to shift that climatological jet poleward, from as far west as western China at D-5d (Fig. 6a) to the northwest US beyond D0 (Fig. 6c).

A poleward shift of the jet similarly shifts the synoptic-scale height anomaly centers 10-15˚ poleward. A broad anomalous upper-level trough over the Gulf of Alaska and far eastern Russia contrasts with a zonally elongated anomalous ridge along the latitude of the climatological jet near the jet exit region at D-5d (Fig. 6a),

helping to shift the pattern poleward and intensify the jet between the anomalous trough and ridge. The anomalous trough retrogrades across the Aleutian Islands and intensifies throughout the 10-day composite (Fig. 6c, e). In turn, anomalous upper-level winds expand around the base of the trough and toward the west coast of North America and are associated with the intensification of the downstream ridge over Hudson Bay by D+5d (Fig. 6e). The low-level anomalous cyclone associated with the upper-level anomalous trough retrogrades with the upper trough between D0 and D+5d and reinforces the low-level cold (warm) temperature anomalies present over the Bering Sea (central Canada; Fig. 6d, f). While the cold temperature anomalies over far eastern Russia peak in excess of -4˚C at D+5d (Fig. 6f), the corresponding warm anomalies over central Canada are enhanced by southwesterly winds downsloping off the Rocky Mountains on the southwest side of the Aleutian cyclone and peak in excess of +8˚C at D+5d. This anomalous warmth continues to impact North America for several days beyond the D+5d lag (not shown).

Upstream of the North Pacific, a weak and nearly stationary anomalous ridge is present near the entrance region of the climatological jet at 110˚E (D-5d, Fig. 6a). This anomalous ridge is maintained throughout the 10 day composite, suggesting its presence may be related to a persistent forcing such as deep convection. An additional notable upstream precursor appears as an anomalous shortwave trough near the Korean peninsula at D-5d (Fig. 6a). While this trough may initially amplify southerly flow out of lower latitudes, it becomes indistinguishable by D0 (Fig. 6c).

d. Equatorward shift (negative TE-EOF 2)

The upper-level zonal wind pattern associated with the equatorward shift mode (negative phase of TE-EOF 2) is more difficult to interpret. The primary zonal wind anomalies in the composite straddle the climatological jet exit region with enhanced westerlies located on the southern periphery with a stronger region of reduced westerlies to the north (Fig. 7a, c, f). This structure is similar to but opposite that of the positive phase of TE-EOF 2 and suggests the appropriate description for this pattern is "equatorward shift". While such a description allows for a convenient consistency of nomenclature, an anomalous enhancement of upper-level zonal winds over Alaska and eastern Russia is of equal or greater magnitude than the enhanced westerly flow in the subtropics and may instead represent another branch of the jet stream at high latitude (Fig. 7a, c, e). A negative zonal wind anomaly in a similar location does not characterize the poleward shifted jet events (Fig. 6a, c, e), providing a notable asymmetry between the positive and negative phases of TE-EOF 2.

The equatorward shift mode is comprised of anomalous westerly zonal wind along 20°N latitude in the central Pacific throughout the 10-day composite, with the maximum westerly anomaly over the Hawaiian Islands (Fig. 7a, c, e). This anomalous jet extends eastward and connects with an anomalous jet over central North America, creating a link between the enhanced equatorward-shifted subtropical Pacific jet and the climatological jet stream over Mexico and the United States at D0 and D+5d (Fig. 7c, e). A broad anomalous trough dominates the flow over the western United States and central Canada and acts in concert with a weak anomalous ridge in the southeast United States to enhance the upper winds

between the two anomaly centers. The upper trough is associated with remarkable cold anomalies at 850 hPa over much of Canada (Fig. 7b, d, f). The magnitude of these anomalies increases dramatically between D-5d and D0 (Fig. 7b, d) though the underlying physical mechanism driving the local temperature tendencies is not immediately clear. Some of the local temperature decrease is undoubtedly associated with cold advection in northwesterly low-level flow that originates in northern Alaska and is associated with the intensifying low-level anticyclone over the Aleutian Islands (Fig. 7b, d).

Over the central North Pacific, a strong anomalous upper-level ridge broadly dominates north of 40˚N and serves to enhance the jet stream on its polar edge, north of 60˚N (Fig. 7a, c, e). The cross-arctic flow associated with such a jet is also represented at the 850-hPa level and likely contributes to the anomalous low-level cold in North America at D0 (Fig. 7d) and D+5d (Fig. 7f), despite only weak cold anomalies over Siberia and the Arctic Sea at D-5d. South of this ridge, a broad region of anomalously low upper-level heights is present south of the climatological jet near its exit region and may represent broad upper troughs digging into the subtropics across a range of longitudes in a manner similar to that observed in jet retraction cases (e.g. Fig. 5a, c, e). The position is reminiscent of where Kona lows form in conjunction with retracted jet cases (e.g. Otkin and Martin 2004) and any such trough may weakly enhance the subtropical jet to the south of the trough in this region.

The upstream patterns over Asia are diffuse with no clear-cut synoptic-scale anomalies at D-5d or D0 at upper levels (Fig. 7a, c), suggesting either that the

equatorward shift mode may be triggered by contrasting synoptic-scale setups that cancel out in a composite analysis or that there are not any clear cut Asian mid-latitude precursors to these equatorward-shifted jet cases.

5. Tropical convection composites

Although the results of certain composites often hint at the role of tropical convection in building low-latitude anomalous ridges, such inferences are unsupported without examining proxies of the convection itself. Figures 8 and 9 present OLR composites calculated as previously for each sign of each TE-EOF. OLR is often utilized as a proxy for cold cloud tops associated with deep convection in the tropics and subtropics and is useful in the construction of composites due to its long, homogenous period of record. The OLR composites for the extension mode (Fig. 8a, c, e) and the equatorward shift mode (Fig. 9b, d, f) show little in the way of anomalous tropical convection with no apparent large-scale organization.

Anomalous tropical convection appears in the retraction composite over the eastern Indian Ocean and maritime continent (Fig. 8b, d, f) and appears to move slowly eastward across the 10-day window of the composite. The eastward phase speed of this convection appears similar to or slightly slower than that of convection associated with the Madden-Julian Oscillation (MJO; Madden and Julian 1971, Zhang 2005), which contrasts with the stationary nature of convection found with the retraction mode in Jaffe et al. (2011). The role of this convection in fostering a retraction of the North Pacific jet is not immediately apparent. The second region of convection in the central and eastern tropical North Pacific is consistent with the

484 OLR composite from Jaffe et al. (2011; specifically their Day 10 composite [their Fig.
485 12e] and our D+5d; Fig. 8f) near the Hawaiian Islands, although twice as intense as
486 that found by Jaffe et al. Convection in this location is consistent with the presence
487 of the low-latitude trough that can be noted in the retraction composites (Fig. 5b, d,
488 f).

489 Significant tropical convection anomalies are evident in the poleward shift
490 composite (Fig. 9a, c, e) over Southeast Asia and the maritime continent and are of a
491 larger magnitude than those observed in a similar location in association with the
492 retraction mode. These negative OLR anomalies also appear to remain nearly
493 stationary or move slowly eastward similar to convection associated with the MJO.
494 It is interesting to note that these convective anomalies move eastward at
495 approximately the same speed as the anomalies associated with the retracted jet
496 events (Fig. 8b, d, f), roughly 2° day^{-1}. The quasi-stationary or slow-moving nature of
497 these convective anomalies enables the imposition of persistent forcing on the mid-
498 latitude flow patterns which can impact both the north Pacific jet as well as
499 locations downstream (e.g. Kiladis and Weickmann 1992, Higgins et al. 2000). The
500 broad low-latitude upper-level anomalous ridge in the entrance region of the
501 poleward shift composite (Fig. 6a, c, e) may be a manifestation of upper-level
502 convective outflow in this location that appears to make systematic contributions to
503 the poleward shift of the jet.

504 Finally, it is worth noting that the large region of anomalously high OLR in
505 the eastern Pacific on the equatorward side of the extended jet's exit region (Fig. 8 a,
506 c, e) is coincident with the subsiding branch of the thermally indirect circulation

associated with the extended jet. This OLR anomaly intensifies throughout the 10-day composite (Fig. 8c, e). Farther north, the rising branch of the thermally indirect circulation likely enhances convection in the region of anomalously low OLR off the west coast of the United States at D0 (Fig. 8c).

6. Discussion

TE-EOF analysis reveals the details of the synoptic-scale evolutions associated with the leading modes of North Pacific jet stream variability. While the analysis presented here is consistent with previous work by Schubert and Park (1991), Athanasiadis et al. (2010), and Jaffe et al. (2011), TE-EOF analysis provides an additional component of temporal coherence to analyses of the large-scale environments characteristic of extremes in the leading modes of variability, and thus points to both upstream precursors and downstream impacts.

The two primary modes of variability presented here consist of 1) the jet in either an extended or retracted state or 2) a poleward or equatorward shift of the jet exit region. While previous studies on North Pacific jet variability focused on the transition into a retracted state (Jaffe et al. 2011) and the instantaneous state of the jet in any given mode (Athanasiadis et al. 2010), the TE-EOF technique identifies the evolution of the two phases of each mode of variability centered on the peak intensity of each phase. By design, the extension/retraction and latitudinal shift modes reach their greatest extents at D0 and so employment of the TE window, which includes some of the increase toward and decline away from such peaks, reveals new details regarding the corresponding flow evolutions.

530 Composites constructed based upon high-amplitude events in the TE-PC time
531 series constitute a notable improvement in the temporal coherence of the associated
532 mid-latitude signals compared to composites constructed with traditional EOFs (e.g.
533 Jaffe et al. 2011). The growth of the positive zonal wind anomalies throughout the
534 TE window for the extended jet (Fig. 4) mode draws attention to the role of the
535 anomalous trough that intensifies and moves eastward throughout the following 10
536 days (Figs. 4a, c, e). This trough appears to be central to the development and
537 intensification of the zonal wind anomalies that constitute an extended jet stream,
538 and expanding these composite analyses farther back in time may allow for better
539 identification of such precursor features and their evolution over several the days
540 prior to the central time of the TE window. Similar extension of these composite
541 analyses may provide additional insights into the nature of characteristic precursors
542 of high-amplitude events for all four phases of jet variability. The utility of such
543 long-range composite signals is not yet established and merits further examination.
544 However, armed with a physical understanding of the precursors that drive changes
545 in the North Pacific jet, medium-range forecasters may be better able to combine
546 anticipation of jet variability with knowledge of the associated downstream impacts
547 to improve large-scale forecasts into week two over much of North America.
548 The composite analyses of extended and retracted jets (Figs. 4 and 5) contain
549 elements consistent with the surge phase of the East Asian Winter Monsoon
550 (EAWM; Chang and Lau 1980). At D-5d of the extended jet composite (Fig. 4b), the
551 large area of anomalous low-level cold air over eastern China and the northern
552 South China Sea appears in a location consistent with a well-developed cold surge

553 described by Chang and Lau (1980). Such cold air outbreaks were identified as a
554 possible precursor to jet extension events by Jaffe et al. (2011) and may play a role
555 in the subsequent evolution of extended jets.

556 Within these composite analyses, consistent high-amplitude impacts were
557 noted downstream over North America in the days after the peak in the respective
558 jet mode. For TE-EOF 1, the jet extension (retraction) mode is associated with a
559 large region of low-level warmth (cold) over much of Alaska and western Canada at
560 D0 (Fig. 4d, 5d), with temperature anomalies in excess of 4˚C magnitude. These
561 anomalies suggest such weather might be a common downstream impact of each
562 TE-EOF 1 phase. Similarly, the phases of TE-EOF 2 are associated with even stronger
563 downstream impacts over North America, with both poleward and equatorward
564 shift events leading to low-level temperature anomalies in excess of 8˚C. Neither of
565 these anomalies are of high magnitude prior to D-5d (Fig. 6b, 7b), but rather
566 intensify over North America as the shift of the jet exit region maximizes (at D0).
567 High magnitude temperature anomalies are maintained through D+5d (Fig. 6f, 7f)
568 and beyond for up to an additional five days (not shown), suggesting that latitudinal
569 shifts of the jet exit region (TE-EOF 2) may affect the downstream weather over
570 North America more significantly than jet extensions or retractions (TE-EOF 1).

571 Of the four phases associated with the two modes of variability discussed
572 here, slow-moving and potentially organized tropical convection may play a
573 significant role in two of them. A more complete analysis of the mid-latitude and
574 tropical interactions that lead to these variations in the jet would serve to provide
575 additional insight into the forcing behind such patterns, but is beyond the scope of

this study. The task of identifying such tropical-extratropical interactions has been partially addressed in cases of recurving TCs interacting with the jet stream (e.g. Archambault et al. 2013), but remains a challenge for less organized episodes of persistent deep convection, which are substantially more common phenomenon throughout the tropics and subtropics. The leading modes of jet variability broadly describe the most common evolutions of the North Pacific jet stream, implying a commonplace occurrence such as non-TC convection (e.g. garden-variety as well as MJO- and ENSO-driven) may play a more frequent and significant role in modulating such North Pacific jet variability.

Finally, since the analyses presented here are based upon identification of the dates of *maximum* extension, retraction, and shift, the leading modes identify, for instance, the state of the jet *being extended* rather than the *process of extension*. Thus, the transitions to and from these leading modes, while partially addressed by the lagged composite analysis, merit additional study. Similarities between the jet extension and poleward shift composites (the 850 hPa Gulf of Alaska cyclone and downstream warmth; Figs. 4 and 6) and the jet retraction and equatorward shift composites (the 850 hPa Gulf of Alaska ridge and downstream cold; Figs. 5 and 7) suggest that the leading modes, while mathematically independent, are not physically independent. Thus, examination of the nature of transitions between the phases of each mode promises additional insight into the preferred evolutions of the North Pacific jet stream.

7. Acknowledgements

599 The authors would like to acknowledge the National Science Foundation for
600 their support on this project via grant number AGS-1265182.
601

602 **List of figure captions**

603 Figure 1. Comparison of a traditional PC, a traditional PC with a 10-day smoother,
604 and a TE-PC for the NDJFM 2009-2010 season for the leading mode (top) and
605 second leading mode (bottom) of variability. PCs correspond to EOFs of 250 hPa
606 zonal wind speed over the North Pacific.

607 Figure 2. TE-EOF 1 (extension/retraction) of the 250 hPa zonal wind over the North
608 Pacific. EOF regressed back onto anomaly data is shaded (m s^{-1}; per color bar).
609 Climatological zonal wind is contoured in black starting at 20 m s^{-1}. Top panel (D-
610 5d) represents the TE-EOF pattern at the beginning of the 10-day TE window;
611 middle panel (D0) represents the pattern halfway through the TE window; bottom
612 panel (D+5d) represents the pattern at the end of the TE window.

613 Figure 3. As in Fig. 2 but for TE-EOF 2 (meridional shift) of the 250 hPa zonal wind
614 over the North Pacific.

615 Figure 4. Composite of cases where PC of TE-EOF 1 was positive and was greater
616 than 1.5 sigma, representing jet extension cases. D0 is defined as the midpoint of the
617 10-day window, where D-5d (D+5d) is the beginning (end) point. Left plots (a, c, e)
618 show anomalies of 250 hPa zonal wind (shaded per color bar), heights (dashed
619 every 50 m), and vector winds (per reference vector). Right plots (b, d, f) include
620 anomalies of 850 hPa temperature (shaded per color bar) and heights (dashed

621 every 20 m). Both plots show the climatological zonal wind in black contours
622 starting at 30 m s^{-1}. Composite sample size = 40.
623 Figure 5. As in Fig. 4 for cases where the PC of TE-EOF 1 was less than -1.5 sigma,
624 representing jet retraction cases. Composite sample size = 40.
625 Figure 6. As in Fig. 4 for cases where the PC of TE-EOF 2 was greater than 1.5 sigma,
626 representing poleward shift cases. Composite sample size = 36.
627 Figure 7. As in Fig. 4 for cases where the PC of TE-EOF 2 was less than -1.5 sigma,
628 representing equatorward shift cases. Composite sample size = 45.
629 Figure 8. Composites of OLR (shaded, per color bar) calculated as in Fig. 4 and Fig. 5
630 for jet extension (a, c, e) and jet retraction cases (b, d, f), respectively, from TE-EOF
631 1. Number of cases are consistent with the respective previous composites.
632 Figure 9. As in Fig. 8 for poleward shift (from Fig. 6; a, c, e) and equatorward shift
633 (Fig. 7; b, d, f) jet cases from TE-EOF 2. Number of cases are consistent with the
634 respective previous composites.
635

636 **References**

637 Archambault, H. M., L. F. Bosart, D. Keyser, and J. M. Cordeira, 2013: A Climatological
638 Analysis of the Extratropical Flow Response to Recurving Western North
639 Pacific Tropical Cyclones. *Mon. Wea. Rev.*, **141**, 2325–2346.
640 doi: http://dx.doi.org/10.1175/MWR-D-12-00257.1
641 Athanasiadis, P. J., J. M. Wallace, and J. J. Wettstein, 2010: Patterns of Wintertime Jet
642 Stream Variability and Their Relation to the Storm Tracks*. *J. Atmos. Sci.*, **67**,
643 1361–1381. doi: http://dx.doi.org/10.1175/2009JAS3270.1

644 Chang, C-P., and K. M. W. Lau, 1980: Northeasterly Cold Surges and Near-Equatorial
645 Disturbances over the Winter MONEX Area During December 1974. Part II:
646 Planetary-Scale Aspects. *Mon. Wea. Rev.*, **108**, 298–312.
647 doi: http://dx.doi.org/10.1175/1520-
648 0493(1980)108<0298:NCSANE>2.0.CO;2
649 Chu, P., A. J. Nash, and F. Porter, 1993: Diagnostic Studies of Two Contrasting
650 Rainfall Episodes in Hawaii: Dry 1981 and Wet 1982. *J. Climate*, **6**, 1457–
651 1462. doi: http://dx.doi.org/10.1175/1520-
652 0442(1993)006<1457:DSOTCR>2.0.CO;2
653 Eichelberger, S. J., and D. L. Hartmann, 2007: Zonal Jet Structure and the Leading
654 Mode of Variability. *J. Climate*, **20**, 5149–5163.
655 doi: http://dx.doi.org/10.1175/JCLI4279.1
656 Hannachi, A., 2004: A primer for EOF analysis of climate data. Available online at
657 http://www.met.reading.ac.uk/~han/Monitor/eofprimer.pdf.
658 Higgins, R. W., J-K. E. Schemm, W. Shi, and A. Leetmaa, 2000: Extreme Precipitation
659 Events in the Western United States Related to Tropical Forcing. *J.*
660 *Climate*, **13**, 793–820. doi: http://dx.doi.org/10.1175/1520-
661 0442(2000)013<0793:EPEITW>2.0.CO;2
662 Jaffe, S. C., J. E. Martin, D. J. Vimont, and D. J. Lorenz, 2011: A Synoptic Climatology of
663 Episodic, Subseasonal Retractions of the Pacific Jet. *J. Climate*, **24**, 2846–
664 2860. doi: http://dx.doi.org/10.1175/2010JCLI3995.1

665 Kalnay, E., and co-authors, 1996: The NCEP/NCAR 40-year reanalysis project. *Bull.*
666 *Amer. Meteor. Soc.*, **77**, 437–471. doi: http://dx.doi.org/10.1175/1520-
667 0477(1996)077<0437:TNYRP>2.0.CO;2
668 Kiladis, G. N. and K. M. Weickmann, 1992: Circulation anomalies associated with
669 tropical convection during northern winter. *Mon. Wea. Rev.*, **120**, 1900–1923.
670 doi: http://dx.doi.org/10.1175/1520-
671 0493(1992)120<1900:CAAWTC>2.0.CO;2
672 Koteswaram, P., 1953: An analysis of the high tropospheric wind circulation over
673 India in winter. *Indian J. Meteor. Geophys.*, **4**, 13-21.
674 Lewis, J. M., 2003: Ooishi's Observation: Viewed in the Context of Jet Stream
675 Discovery. *Bull. Amer. Meteor. Soc.*, **84**, 357–369.
676 doi: http://dx.doi.org/10.1175/BAMS-84-3-357
677 Liebmann, B., and C. A. Smith, 1996: Description of a complete (interpolated)
678 outgoing longwave radiation dataset. *Bull. Amer. Meteor. Soc.*, **77**, 1275–1277.
679 Loewe, F., and U. Radok, 1950: A meridional aerological cross section in the
680 southwest Pacific. *J. Meteor.*, **7**, 58–65. doi: http://dx.doi.org/10.1175/1520-
681 0469(1950)007<0058:AMACSI>2.0.CO;2
682 Madden, R. A. and P. R. Julian, 1972: Description of Global-Scale Circulation Cells in
683 the Tropics with a 40–50 Day Period. *J. Atmos. Sci.*,**29**, 1109–1123.
684 doi: http://dx.doi.org/10.1175/1520-
685 0469(1972)029<1109:DOGSCC>2.0.CO;2
686 _____, and _____, 1994: Observations of the 40–50-day tropical oscillation. *Mon.*
687 *Wea. Rev.*, **122**, 814-837.

688 Mohri, K., 1953: On the fields of wind and temperature over Japan and adjacent
689 waters during winter of 1950–1951. *Tellus,* **5**, 340–358.
690 Namias, J. and P. F. Clapp, 1949: Confluence theory of the high tropospheric jet
691 stream. *J. Meteor.*, **6**, 330–336. doi: http://dx.doi.org/10.1175/1520-
692 0469(1949)006<0330:CTOTHT>2.0.CO;2
693 NCAR Command Language (Version 6.3.0) [Software]. (2015). Boulder, Colorado:
694 UCAR/NCAR/CISL/TDD. http://dx.doi.org/10.5065/D6WD3XH5
695 Newton, C. W., 1954: Frontogenesis and frontolysis as a three-dimensional process.
696 *J. Meteor.*, **11**, 449-461.
697 Otkin, J. A. and J. E. Martin, 2004: The Large-Scale Modulation of Subtropical
698 Cyclogenesis in the Central and Eastern Pacific Ocean. *Mon. Wea. Rev.*, **132**,
699 1813–1828. doi: http://dx.doi.org/10.1175/1520-
700 0493(2004)132<1813:TLMOSC>2.0.CO;2
701 Palmén, E., 1951: The role of atmospheric disturbances in the general circulation.
702 *Quart. J. Royal Meteor. Soc.*, **77**, 337-354. doi:
703 http://dx.doi.org/10.1002/qj.49707733302
704 Roundy, P. E., and C. J. Schreck III, 2009: A combined wave-number–frequency and
705 time-extended EOF approach for tracking the progress of modes of large-
706 scale organized tropical convection. *Quart. J. Royal Meteor. Soc.*, **135**, 161-
707 173.
708 Schubert, S. D. and C. Park, 1991: Low-Frequency Intraseasonal Tropical-
709 Extratropical Interactions. *J. Atmos. Sci.*, **48**, 629–650.

710 doi: http://dx.doi.org/10.1175/1520-
711 0469(1991)048<0629:LFITEI>2.0.CO;2
712 Thompson, D. W. J., and J. M. Wallace, 1998: The arctic oscillation signature in the
713 wintertime geopotential height and temperature fields. *Geophys. Research*
714 *Letters*, **25**, 1297-1300.
715 Wallace, J. M. and D. S. Gutzler, 1981: Teleconnections in the geopotential height
716 field during the Northern Hemisphere winter. *Mon. Wea. Rev.*, **109**, 784–812.
717 doi: http://dx.doi.org/10.1175/1520-
718 0493(1981)109<0784:TITGHF>2.0.CO;2
719 Weare, B. C., and J. S. Nasstrom, 1982: Examples of Extended Empirical Orthogonal
720 Function Analyses. *Mon. Wea. Rev.*, **110**, 481–485.
721 doi: http://dx.doi.org/10.1175/1520-
722 0493(1982)110<0481:EOEEOF>2.0.CO;2
723 Wheeler, M. C., and H. H. Hendon, 2004: An All-Season Real-Time Multivariate MJO
724 Index: Development of an Index for Monitoring and Prediction. *Mon. Wea.*
725 *Rev.*, **132**, 1917–1932. doi: http://dx.doi.org/10.1175/1520-
726 0493(2004)132<1917:AARMMI>2.0.CO;2
727 Wilks, D. S., 2011: Statistical methods in the atmospheric sciences. Academic Press,
728 676 pp.
729 Yeh, T., 1950: The circulation of the high troposphere over China in the winter of
730 1945-46. *Tellus*, **2**, 173–183.
731 Zhang, C., 2005: Madden-Julian Oscillation. *Rev. Geophys.*, **43**.

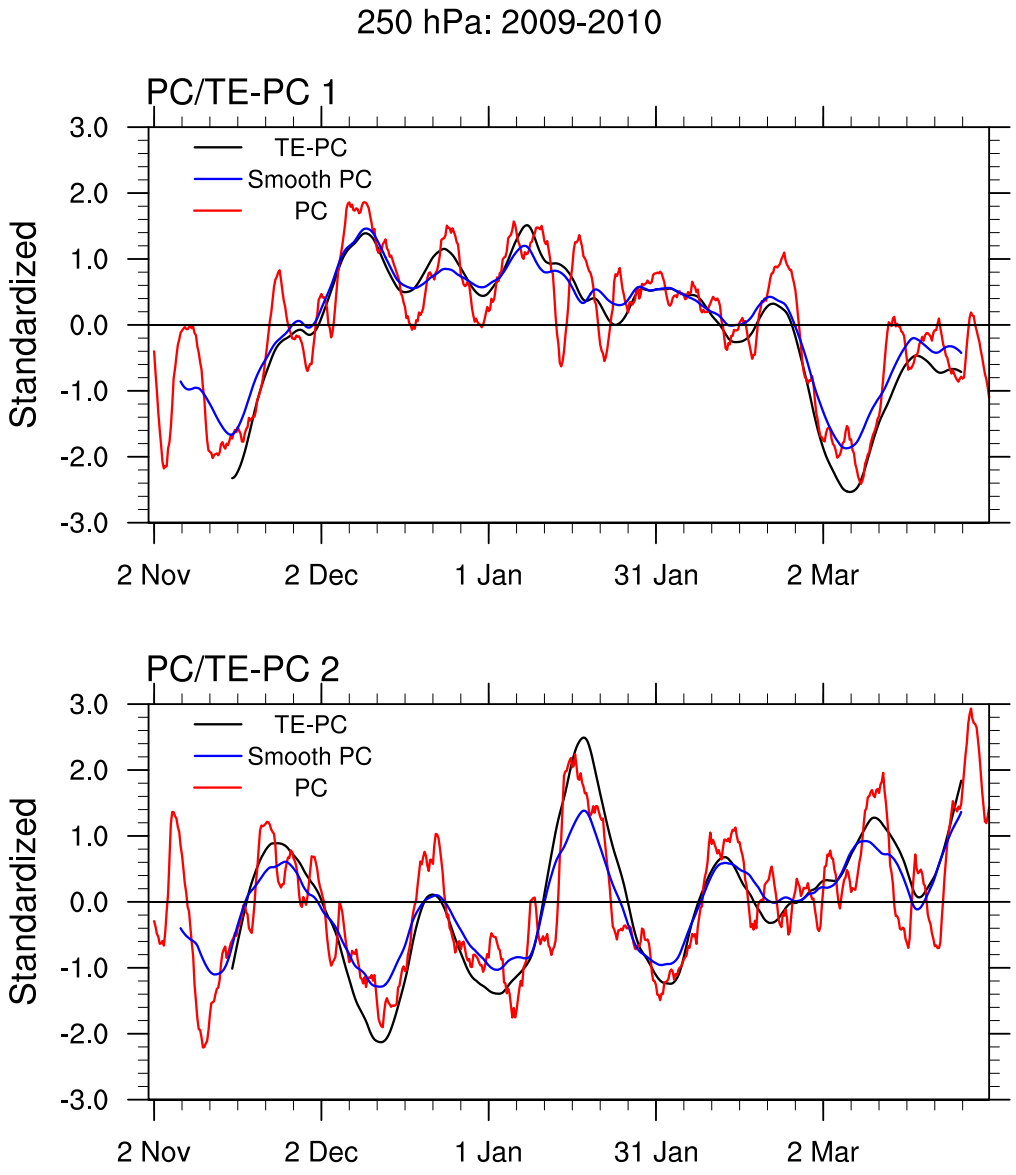

732
733 Figure 1. Comparison of a traditional PC, a traditional PC with a 10-day smoother,
734 and a TE-PC for the NDJFM 2009-2010 season for the leading mode (top) and
735 second leading mode (bottom) of variability. PCs correspond to EOFs of 250 hPa
736 zonal wind speed over the North Pacific.
737

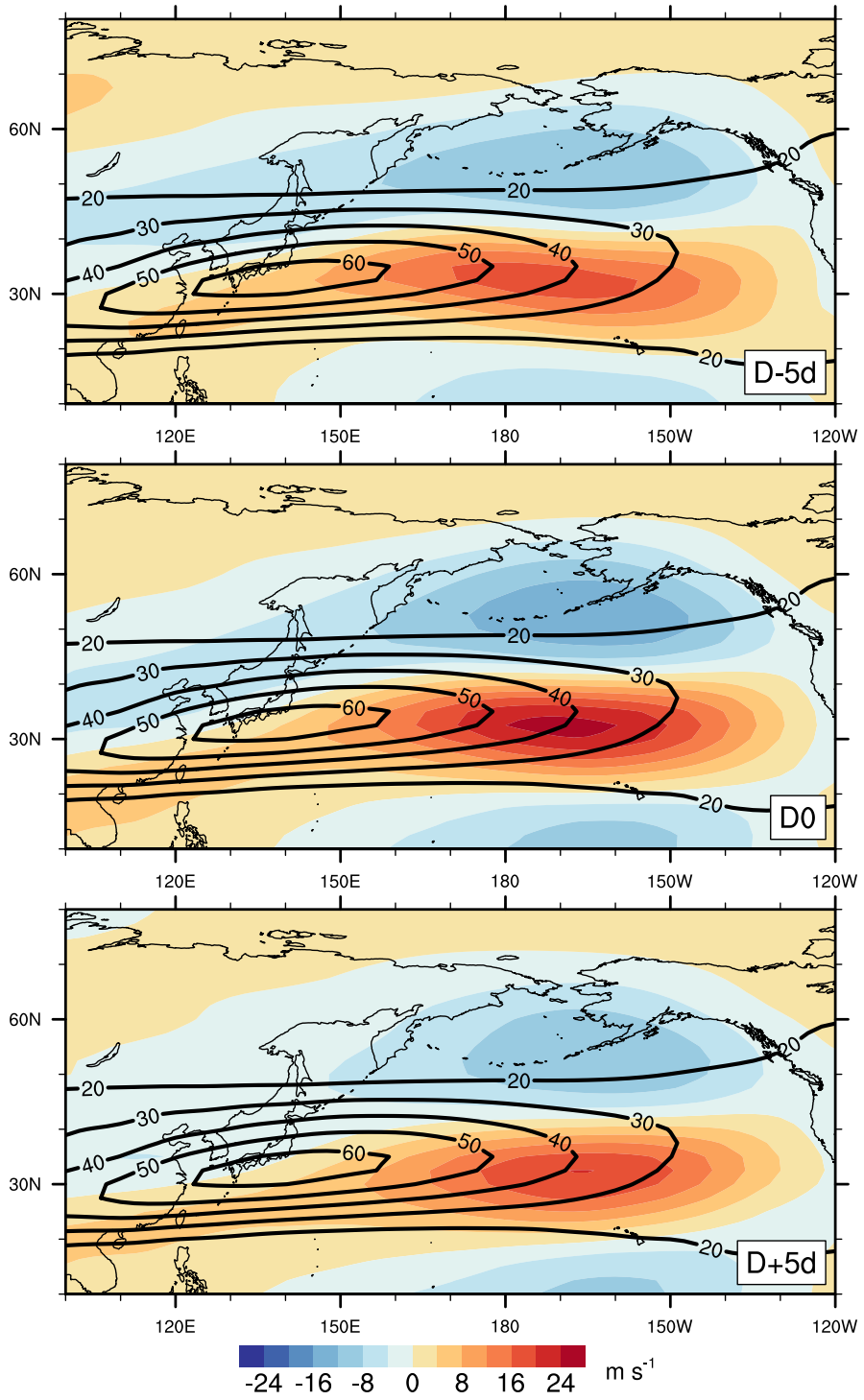

Fig. 2. TE-EOF 1 (extension/retraction) of the 250 hPa zonal wind over the North Pacific. EOF regressed back onto anomaly data is shaded (m s^{-1}; per color bar). Climatological zonal wind is contoured in black starting at 20 m s^{-1}. Top panel (D-5d) represents the TE-EOF pattern at the beginning of the 10-day TE window; middle panel (D0) represents the pattern halfway through the TE window; bottom panel (D+5d) represents the pattern at the end of the TE window.

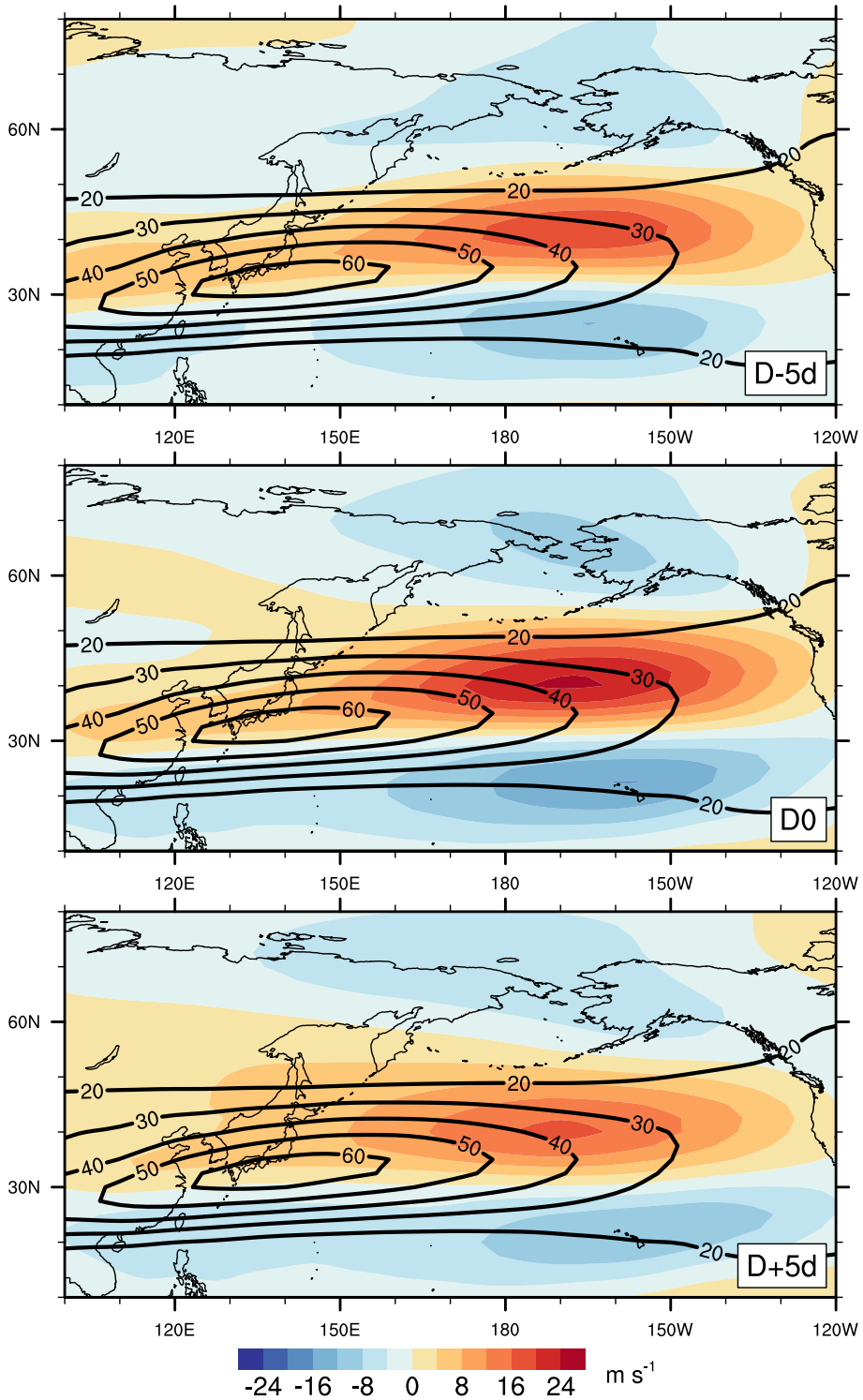

745
746 Fig. 3. As in Fig. 2 but for TE-EOF 2 (meridional shift) of the 250 hPa zonal wind over
747 the North Pacific.

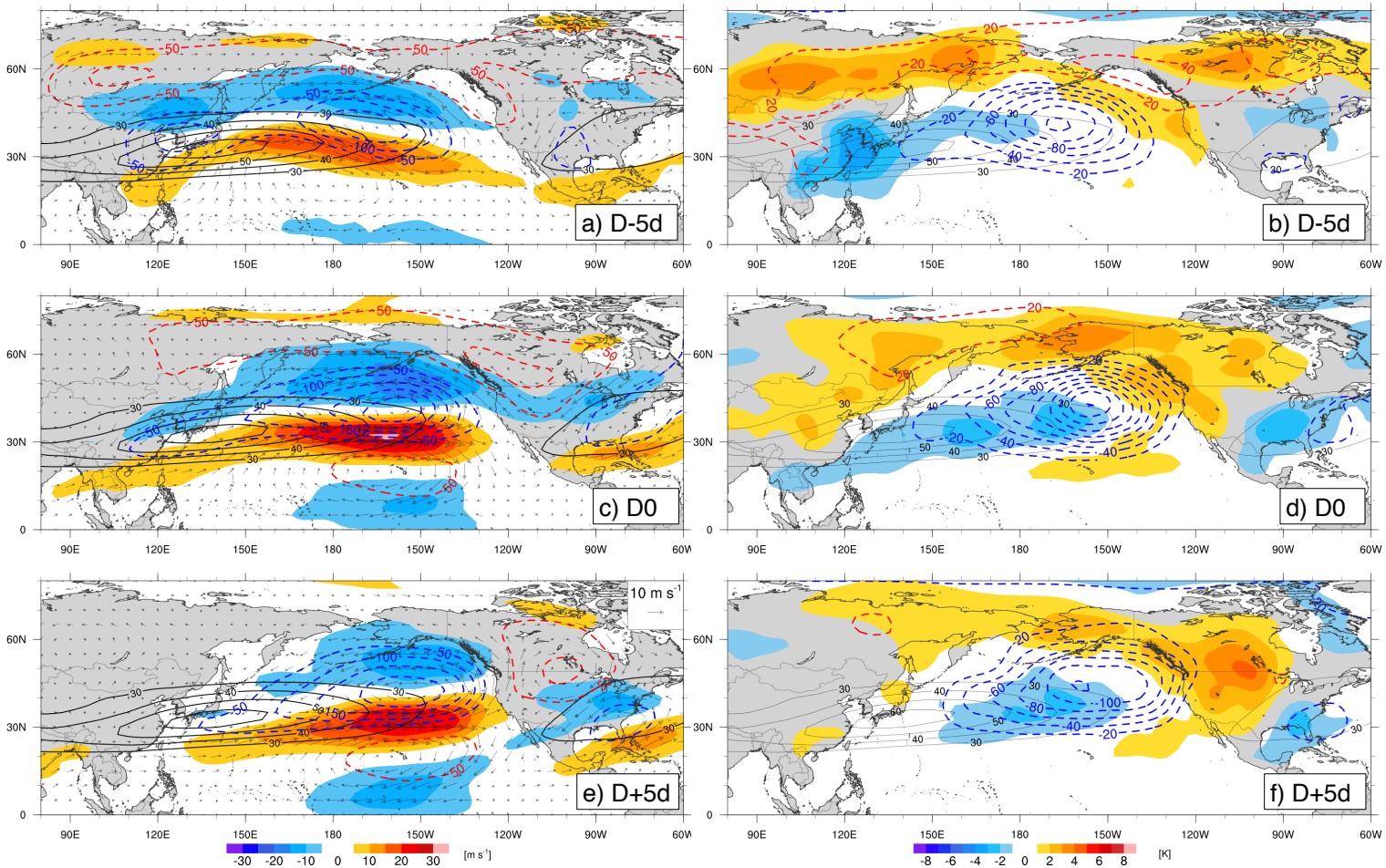

Fig. 4. Composite of cases where PC of TE-EOF 1 was positive and was greater than 1.5 sigma, representing jet extension cases. D0 is defined as the midpoint of the 10-day window, where D-5d (D+5d) is the beginning (end) point. Left plots (a, c, e) show anomalies of 250 hPa zonal wind (shaded per color bar), heights (dashed every 50 m), and vector winds (per reference vector). Right plots (b, d, f) include anomalies of 850 hPa temperature (shaded per color bar) and heights (dashed every 20 m). Both plots show the climatological zonal wind in black contours starting at 30 m s^{-1}. Composite sample size = 40.

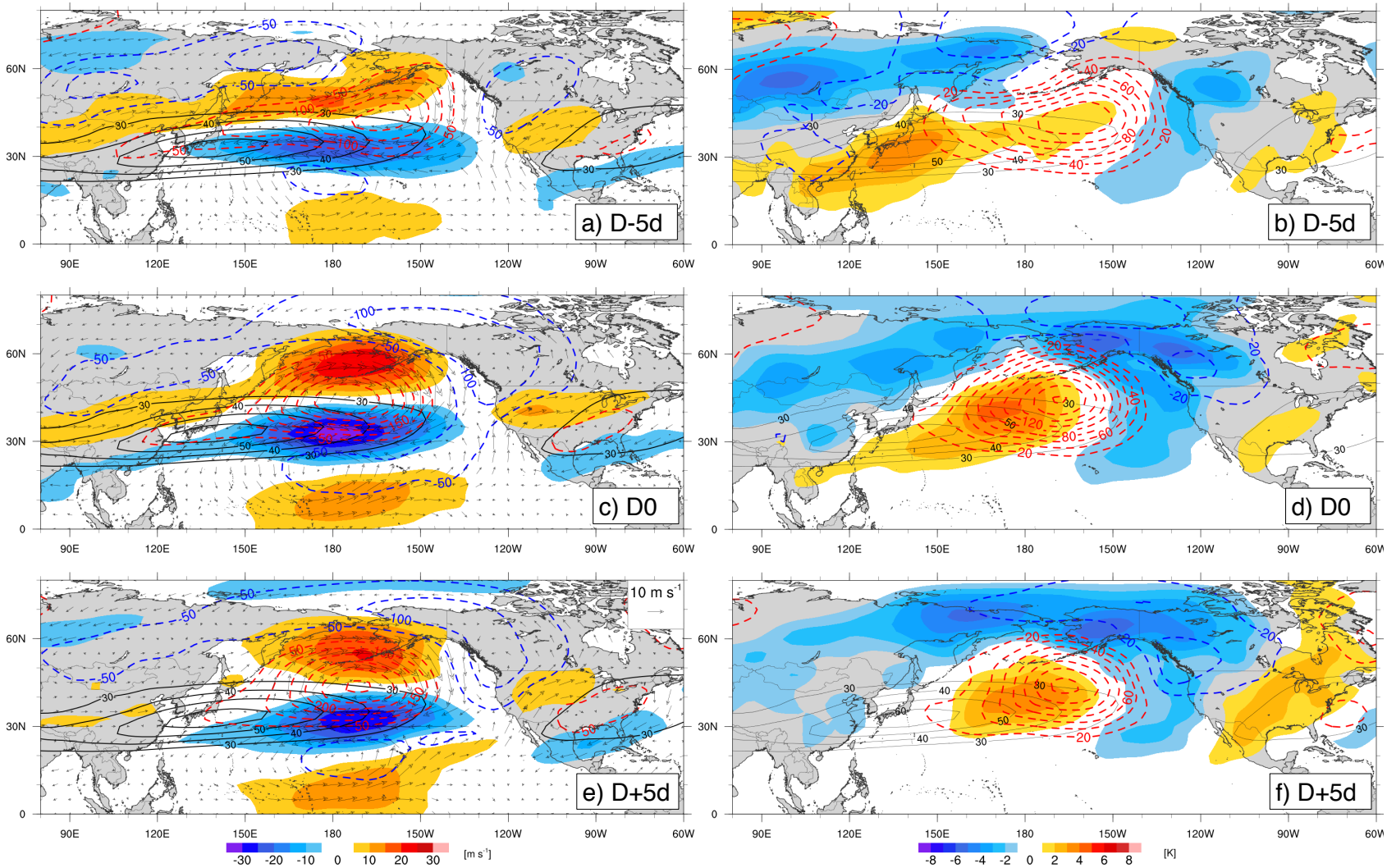

Fig. 5. As in Fig. 4 for cases where the PC of TE-EOF 1 was less than -1.5 sigma, representing jet retraction cases. Composite sample size = 40.

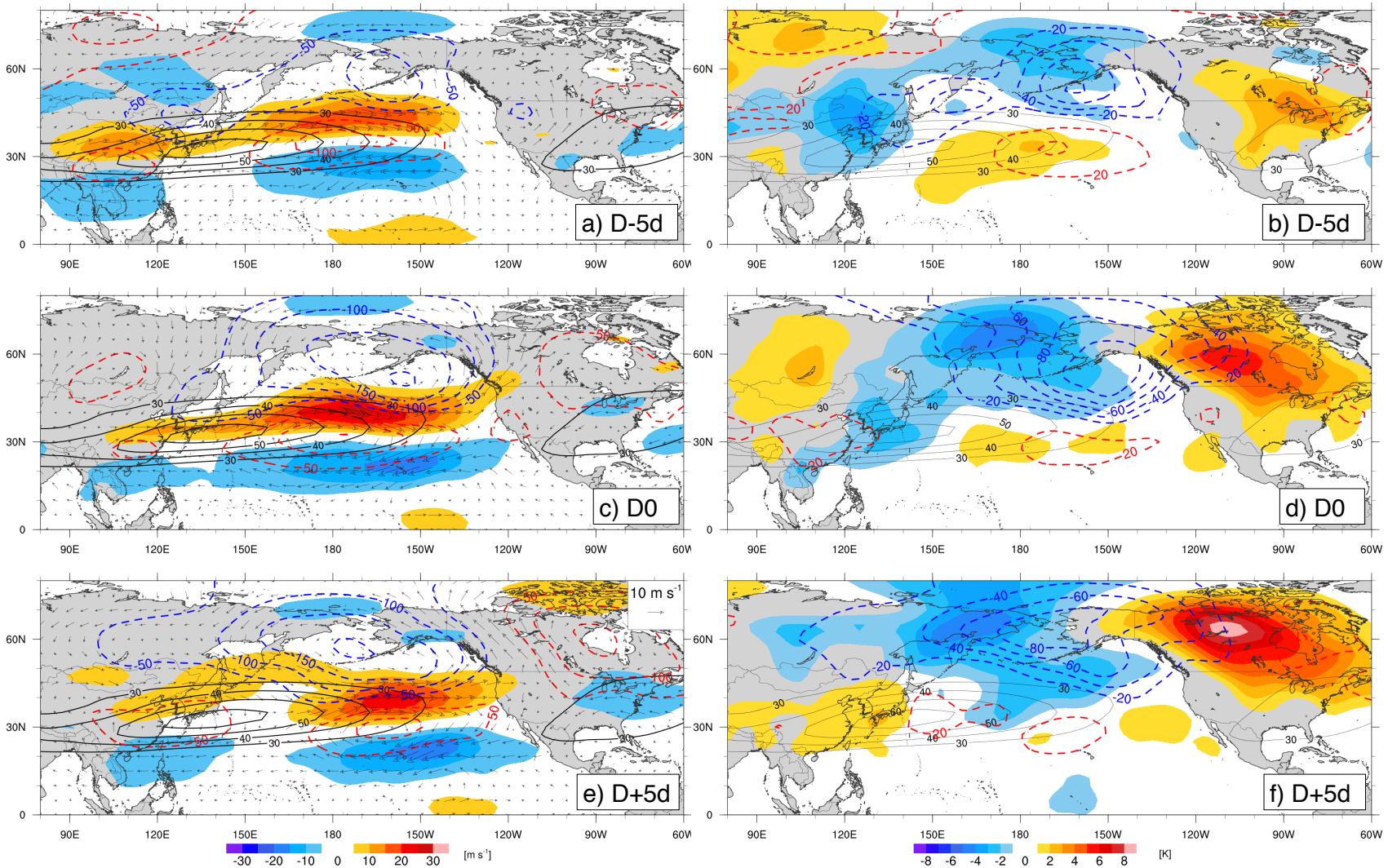

Fig. 6. As in Fig. 4 for cases where the PC of TE-EOF 2 was greater than 1.5 sigma, representing poleward shift cases. Composite sample size = 36.

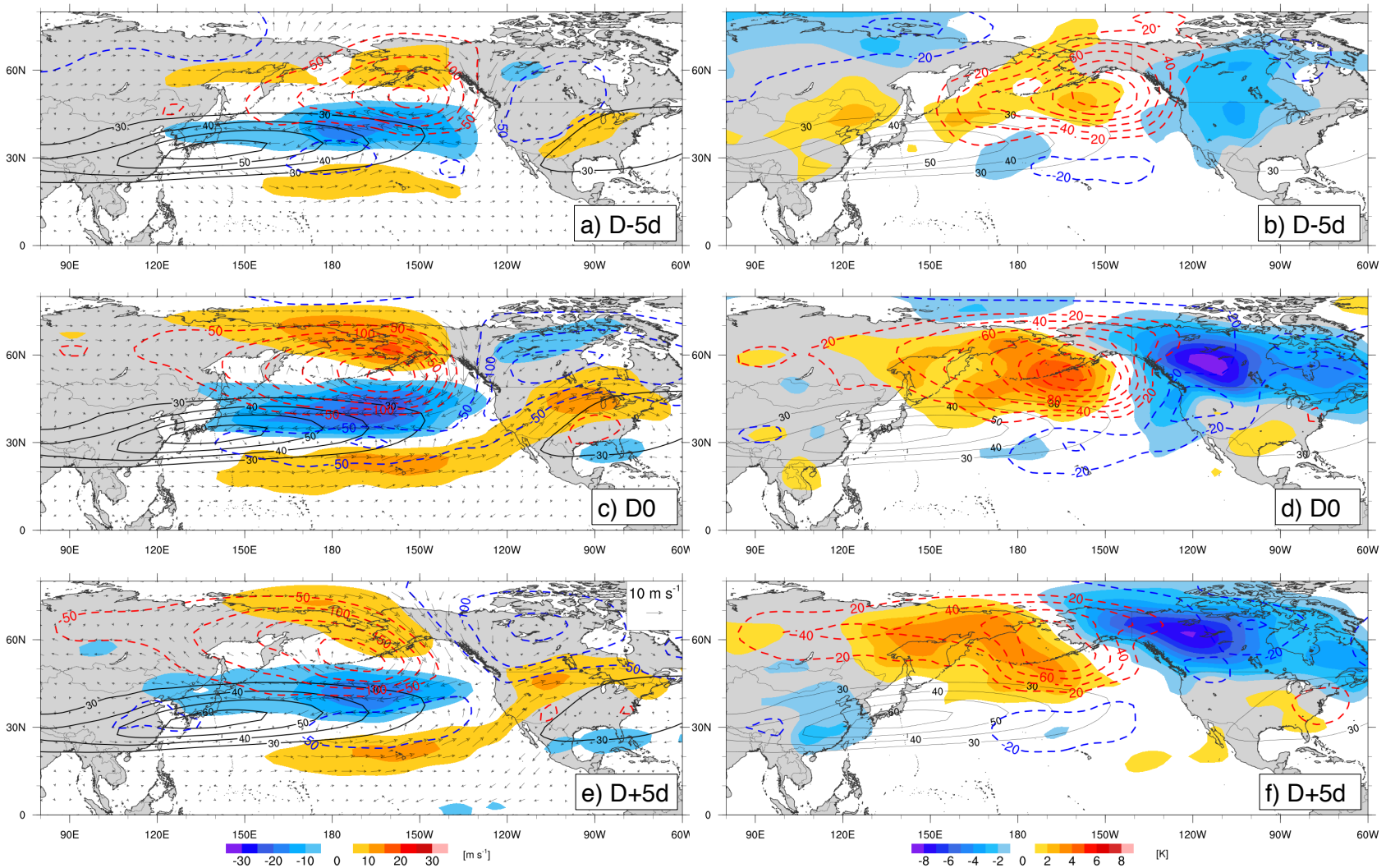

Fig. 7. As in Fig. 4 for cases where the PC of TE-EOF 2 was less than -1.5 sigma, representing equatorward shift cases. Composite sample size = 45.

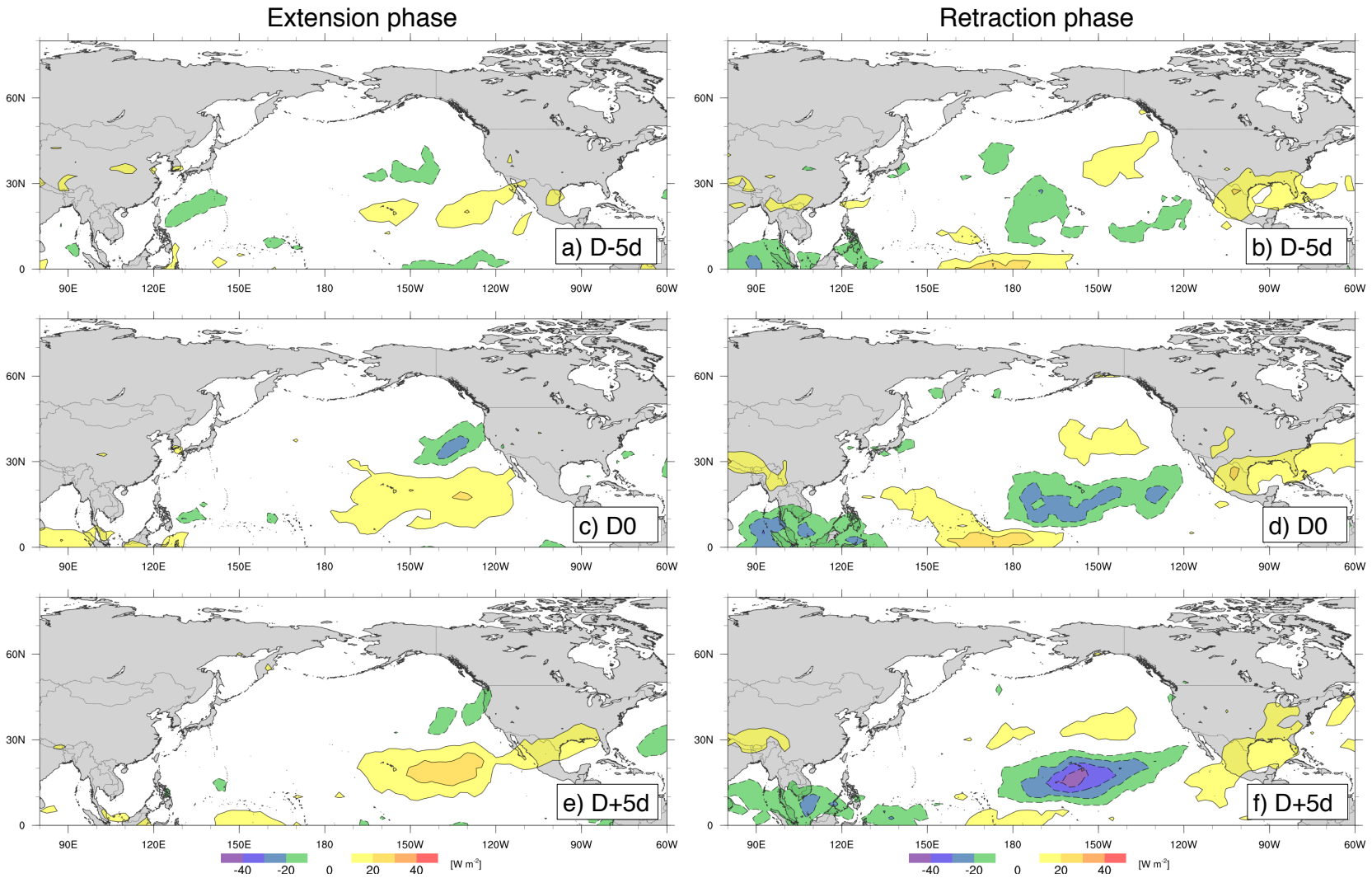

Fig. 8. Composites of OLR (shaded, per color bar) calculated as in Fig. 4 and Fig. 5 for jet extension (a, c, e) and jet retraction cases (b, d, f), respectively, from TE-EOF 1. Number of cases are consistent with the respective previous composites.

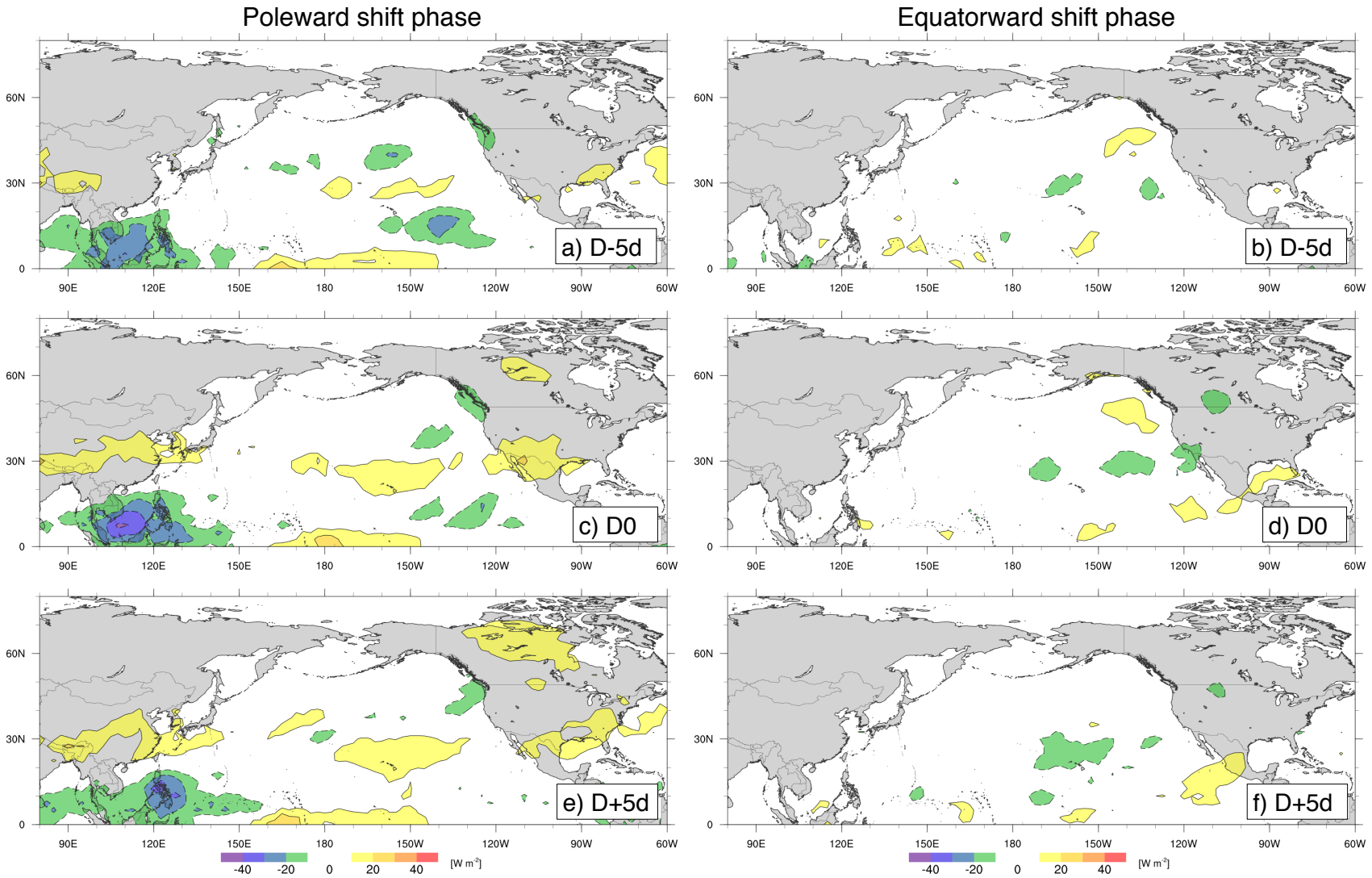

Fig. 9. As in Fig. 8 for poleward shift (from Fig. 6; a, c, e) and equatorward shift (Fig. 7; b, d, f) jet cases from TE-EOF 2. Number of cases are consistent with the respective previous composites.